JOURNAL OF COMPUTATIONAL PHYSICS 40, 345–360 (1981)

Applications of Numerical Conformal Mapping*

DANIEL I. MEIRON AND STEVEN A. ORSZAG

Department of Mathematics, Massachusetts Institute of Technology, Cambridge, Massachusetts 02139

AND

MOSHE ISRAELI

Department of Computer Science, Technion-Israel Institute of Technology, Haifa, Israel

Received July 23, 1980

The application of conformal mapping methods to the solution of free-surface flow problems is considered. Methods of numerical conformal mapping based on Fourier series are extended to handle efficiently problems with time-dependent boundaries. They are shown to be practicable only for moderately distorted geometries. Extensions of the Menikoff–Zemach method to "breaking" geometries are presented. These latter methods are robust at quite large distortions, but degrade prematurely in time-dependent problems at amplitudes smaller than achieved by our recent vortex methods.

1. INTRODUCTION

In this paper, we investigate the application of conformal mapping to the solution of time-dependent potential flow problems, such as Rayleigh–Taylor instability and water waves. We begin by formulating the water wave problem. For two-dimensional, incompressible, irrotational, free-surface flow, the velocity is expressible as $\mathbf{v} = \nabla\phi$, where the potential ϕ satisfies Laplace's equation $\nabla^2\phi = 0$ in the region $y < \eta(x, t)$ beneath the free surface $y = \eta(x, t)$. Since the free surface moves with the fluid,

$$\frac{Dx}{Dt} = \phi_x, \qquad \frac{Dy}{Dt} = \phi_y, \qquad (y = \eta(x, t)), \tag{1.1}$$

where D/Dt is a Lagrangian derivative. Bernoulli's law is satisfied throughout the fluid so that

$$\frac{D\phi}{Dt} = -\eta(x, t) + \frac{1}{2}v^2 - p_s \tag{1.2}$$

at the free surface $y = \eta(x, t)$, where the gravitational acceleration is normalized to

* This work was supported by the Air Force Office of Scientific Research under Grant 77-3405 and the General Hydromechanics Research Program of the Naval Sea Systems Command under Contract N00014-80-C-0127.

0021-9991/81/040345-16$02.00/0

unity and p_s is the applied surface pressure. It is assumed below that the free surface is periodic in x with wavelength 2π.

In order to march forward in time, it is necessary to know $\nabla\phi$ at the free surface. If ϕ is known then its tangential derivative $\partial\phi/\partial s$ is computable but its normal derivative $\partial\phi/\partial n$ must be found by solving Laplace's equation. Green's third formula expresses $\partial\phi/\partial n$ in terms of ϕ:

$$\int_{\partial D} \frac{\partial}{\partial n} \ln|\mathbf{p}-\mathbf{q}|\,\phi(\mathbf{q})\,d\mathbf{q} - \int_{\partial D} \ln|\mathbf{p}-\mathbf{q}|\,\frac{\partial\phi}{\partial n}(\mathbf{q})\,d\mathbf{q} = \pi\phi(\mathbf{p}). \tag{1.3}$$

Here $\mathbf{p}, \mathbf{q}$ are vectors lying on the boundary ∂D of the region D. Equation (1.3) is a linear integral equation of the first kind for the unknown function $\partial\phi/\partial n$. Once $\partial\phi/\partial n$ has been calculated, Eqs. (1.1) and (1.2) may be used to update the free surface and potential.

Numerical solution of (1.3) for $\partial\phi/\partial n$ involves the approximation of its logarithmic kernel by a finite matrix. If the continuous boundary is approximated by N discrete points, the operation count for the solution of the resulting linear system is $O(N^3)$ since the matrix is full. In addition, storage of the matrix requires $O(N^2)$ memory locations. For large N the computational costs are prohibitive.

Our work is motivated by the desire to develop algorithms with decreased operation counts and storage requirements for solving free-surface potential flow problems. We have recently proposed a new vortex method [1, 2] to solve these problems with $O(N)$ memory and $O(N^2)$ operations per time step. In the present paper, two conformal mapping methods are studied. Both require only $O(N)$ memory. The methods discussed in Section 2 require only $O(N \log_2 N)$ operations per time step but are effectively limited to modest surface deformations. In Section 3, modifications of the Menikoff–Zemach method [10] that require $O(N^2)$ operations per time step are introduced. Larger surface deformations can be handled accurately by these latter methods.

2. Conformal Mapping Using Fourier Series

In this Section, numerical methods are developed to compute the conformal map $z(\zeta)$ of the unit disk $|\zeta| \leqslant 1$ onto a simply connected finite region D in the complex-z plane. A map of the unit disk onto a semi-infinite periodic region R: $w = x + iy$, $0 \leqslant x \leqslant 2\pi$, $y < \eta(x)$, is given by

$$w = i \ln z(\zeta), \tag{2.1}$$

where $z(\zeta)$ is a map of the unit disk onto the interior of the region with boundary

$$z = \exp[-ix + \eta(x)].$$

This sequence of conformal maps is depicted in Fig. 1.

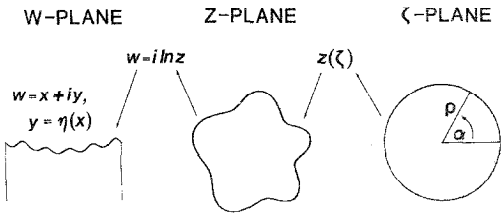

FIG. 1. A schematic plot indicating the sequence of conformal maps used to solve inviscid free-surface flow problems. Here the fluid lies below the interface $y = \eta(x, t)$ as in the water wave problem.

Before proceeding to the discussion of methods to compute the conformal map $z(\zeta)$, we note that knowledge of $z(\zeta)$ allows efficient solution of potential problems in the region R. If $\phi(w)$ is harmonic in R then $\phi(i \ln z(\zeta))$ is harmonic in the unit disk. Therefore, the Dirichlet problem can be solved by Poisson's formula. Also, since conformal maps are angle preserving, the normal derivative $\partial\phi/\partial n$ of ϕ on the boundary of R is related to the radial derivative $\partial\phi/\partial\rho$ of ϕ on $|\zeta| = \rho = 1$:

$$\left.\frac{\partial\phi}{\partial n}\right|_{y=\eta(x)} = \left.\frac{\partial\phi}{\partial\rho}\right|_{\rho=1} \left|\frac{z(\zeta)}{dz/d\zeta}\right|_{\rho=1} \tag{2.2}$$

The derivative $dz/d\zeta$ can not vanish for $|\zeta| \leqslant 1$ if $z(\zeta)$ is single valued.

Let us begin by characterizing the analytic character of $z(\zeta)$ in terms of Fourier series. The boundary values $z(e^{i\alpha})$ of the conformal map $z(\zeta)$ are a periodic function of the angle α on the unit disk so

$$z(e^{i\alpha}) = \sum_{k=-\infty}^{\infty} A_k e^{ik\alpha}. \tag{2.3}$$

The condition that $z(\zeta)$ be analytic is

$$A_k = 0, \qquad k < 0, \tag{2.4}$$

and, in this case, $z(\zeta)$ is given explicitly by

$$z(\zeta) = \sum_{k=0}^{\infty} A_k \zeta^k. \tag{2.5}$$

In other words, an analytic transformation of the unit disk onto a region D is equivalent to a parametrization of ∂D in terms of α such that the Fourier representation of ∂D has only positive frequency components

Now we consider a discrete approximation to the conformal map. Consider the equally spaced discrete points $\alpha_j = \sigma j$ $(j = 0,..., N-1)$, where $\sigma = 2\pi/N$, and the associated points z_j on ∂D. Then z_j can be represented as the finite Fourier series

$$z_j = z(e^{i\sigma j}) = \sum_{-N/2 \leqslant k < N/2} a_k e^{ik\sigma j} \qquad (0 \leqslant j < N). \tag{2.6}$$

It may easily be shown that

$$a_k = A_k + \sum_{p \neq 0} A_{k+pN}. \tag{2.7}$$

One way to determine an approximation to the conformal map $z(\zeta)$ is to require that $a_k = 0$ for $k < 0$. Indeed, if N is large enough that A_k is negligible for $k > N$, then a_k is negigibly small for $k < 0$. This idea may be used to obtain iterative methods [4–8] based on the fast Fourier transform (FFT) to compute the approximate conformal map. These methods typically require $O(N \log_2 N)$ operations per iteration. We note that for any a_k satisfying $a_k = 0$ for $k < 0$, the resulting conformal map

$$\hat{z}(\zeta) = \sum_{0 \leqslant k < N/2} a_k \zeta^k \tag{2.8}$$

satisfies $\hat{z}(e^{i\sigma j}) = z_j$. Thus, the map $\hat{z}$ transforms the N equally spaced points $e^{i\sigma j}$ into points z_j lying on ∂D.

As an alternative to these iterative methods, we have obtained a differential equation which relates the time rate of change of the conformal map to the time rate of change of a moving boundary. This differential equation is well suited to the solution of free-surface flow problems where the solution of the potential problem determines the time rate of change of the free surface.

Let the boundary be represented for all time t by the equation

$$F(z(\alpha, t), \bar{z}(\alpha, t), t) = 0. \tag{2.9}$$

Differentiation of (2.9) with respect to t yields

$$\frac{\partial F}{\partial t} + \frac{\partial F}{\partial z}\frac{\partial z}{\partial t} + \frac{\partial F}{\partial \bar{z}}\frac{\partial \bar{z}}{\partial t} = 0, \tag{2.10}$$

and differentiation with respect to the angle α (see Fig. 1) gives

$$\frac{\partial F}{\partial z}\frac{\partial z}{\partial \alpha} + \frac{\partial F}{\partial \bar{z}}\frac{\partial \bar{z}}{\partial \alpha} = 0. \tag{2.11}$$

The relation

$$\operatorname{Im}\left(\frac{\dfrac{\partial z}{\partial t}}{\dfrac{\partial z}{\partial \alpha}}\right) = \frac{i}{2}\frac{\dfrac{\partial F}{\partial t}}{\dfrac{\partial F}{\partial z}\dfrac{\partial z}{\partial \alpha}} \tag{2.12}$$

is obtained by substituting (2.11) into (2.10). This equation only provides the imaginary part of $(\partial z/\partial t)/(\partial z/\partial \alpha)$. The real part of $(\partial z/\partial t)/(\partial z/\partial \alpha)$ is determined by requiring that it be analytic in the domain described by (2.9).

The right-hand side of (2.12) is real and can be represented by a conjugate symmetric Fourier series:

$$\frac{i}{2}\frac{\overline{\dfrac{\partial F}{\partial t}}}{\dfrac{\partial F}{\partial z}\dfrac{\partial z}{\partial \alpha}} = \mathrm{Re}\left[\sum_{m=0}^{(N-1)/2} b_m \exp(\mathrm{im}\,\alpha)\right].$$

Therefore, analytic continuation of (2.12) gives

$$\frac{\partial z}{\partial t} = i\frac{\partial z}{\partial \alpha}\sum_{m=0}^{(N-1)/2} b_m \exp(\mathrm{im}\,\alpha), \tag{2.13}$$

where

$$\frac{\partial z}{\partial \alpha} = \sum_{k=0}^{(N-1)/2} (ik) a_k \exp ik\alpha. \tag{2.14}$$

The right-hand side of Eq. (2.12) is directly related to the normal velocity of the moving boundary. In Cartesian coordinates

$$F(z, \bar{z}, t) = y - \eta(x, t) \tag{2.15}$$

so

$$\frac{\partial F}{\partial t} = -\frac{\partial \eta}{\partial t}. \tag{2.16}$$

Also,

$$\frac{\partial F}{\partial z}\frac{\partial z}{\partial \alpha} = \frac{1}{2}\left(\frac{\partial F}{\partial x} - i\frac{\partial F}{\partial y}\right)\left(\frac{\partial x}{\partial \alpha} + i\frac{\partial y}{\partial \alpha}\right). \tag{2.17}$$

Substitution of (2.16) and (2.17) into (2.12) gives

$$\mathrm{Im}\left(\frac{\dfrac{\partial z}{\partial t}}{\dfrac{\partial z}{\partial \alpha}}\right) = \frac{\dfrac{\partial \eta}{\partial t}}{\dfrac{\partial x}{\partial \alpha} + \dfrac{\partial \eta}{\partial x}\dfrac{\partial y}{\partial \alpha}}. \tag{2.18}$$

The free-surface condition (1.1) can be written as

$$\frac{\partial \eta}{\partial t} = \frac{\partial \phi}{\partial y} - \frac{\partial \eta}{\partial x}\frac{\partial \phi}{\partial x}. \tag{2.19}$$

Using the decomposition of $\partial\phi/\partial x$ and $\partial\phi/\partial y$ into tangential and normal components

$$\frac{\partial\phi}{\partial y} = \left(\frac{\partial y}{\partial s}\frac{\partial\phi}{\partial s} - \frac{\partial x}{\partial s}\frac{\partial\phi}{\partial n}\right),$$
$$\frac{\partial\phi}{\partial x} = \left(\frac{\partial x}{\partial s}\frac{\partial\phi}{\partial s} + \frac{\partial y}{\partial s}\frac{\partial\phi}{\partial n}\right) \tag{2.20}$$

in (2.18) gives the final result in terms of the polar coordinates ρ and α:

$$\mathrm{Im}\left[\frac{\dfrac{\partial z}{\partial t}}{\dfrac{\partial z}{\partial \alpha}}\right] = -\frac{\partial\phi}{\partial\rho}\bigg|_{\rho=1}\left|\frac{z}{\dfrac{\partial z}{\partial\alpha}}\right|^2. \tag{2.21}$$

An analogous result was obtained using perturbation methods by Kantorovich and Krylov [8].

Eq. (2.21) describes the motion of points following the conformal map of the free surface rather than the Lagrangian or Eulerian paths. Bernoulli's equation (1.2) must also be modified to take this fact into account:

$$\frac{D\phi}{Dt} = -\ln|z| - \frac{1}{2}\left[\left(\frac{\partial\phi}{\partial\rho}\right)^2 + \left(\frac{\partial\phi}{\partial\alpha}\right)^2\right]\left|\frac{z}{\dfrac{\partial z}{\partial\alpha}}\right|^2$$
$$+\frac{\partial\phi}{\partial x}\frac{Dx}{Dt} + \frac{\partial\phi}{\partial y}\frac{Dy}{Dt} - p_s. \tag{2.22}$$

Once the conformal map (2.5) from the unit circle is known, the solution of the Dirichlet problem may be given in terms of a Fourier series

$$\phi(\rho e^{i\alpha}) = \sum_{n=0}^{(N-1)/2}[g_n\rho^n\cos n\alpha + h_n\rho^n\sin n\alpha]. \tag{2.23}$$

On the unit circle ($\rho = 1$) the tangential and normal derivatives are given by

$$\frac{\partial\phi}{\partial\alpha} = \sum_{n=0}^{(N-1)/2}[-ng_n\sin n\alpha + nh_n\cos n\alpha], \tag{2.24}$$

$$\frac{\partial\phi}{\partial\rho} = \sum_{n=0}^{(N-1)/2}[ng_n\cos b\alpha + nh_n\sin n\alpha], \tag{2.25}$$

which are computable using FFTs in $O(N\log_2 N)$ operations.

Now let us summarize the steps involved in marching from time t to $t+\Delta t$ by this method. At time t, the points $\{z_j\}$ and potentials $\{\phi_j\}$ are assumed known. First, the coefficients g_n, h_n in (2.23) are obtained from $\{\phi_j\}$ using an FFT. Next, $\nabla\phi$ is computed on the boundary using (2.24) and (2.25). Then $\{\phi_j\}$ is updated by (2.22)

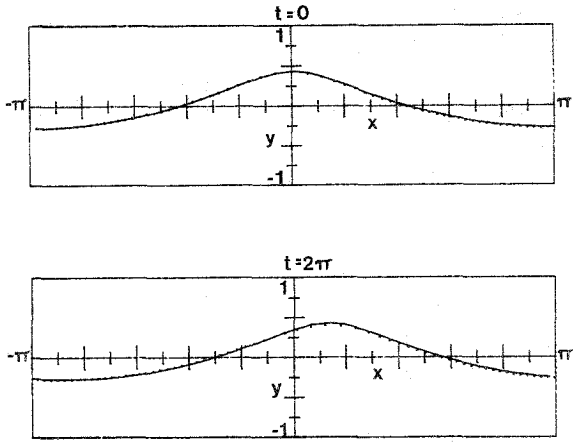

FIG. 2. A plot of the Stokes wave profile at $t = 0$ and at $t = 2\pi$. The amplitude is 80% of the maximum Stokes wave amplitude. The FFT time-dependent mapping equation (2.21) is used with $N = 64$ points. The dots indicate the numerically computed position of the interface. The solid line is obtained from Padé summation of the perturbation series for Stokes waves.

and $\{z_j\}$ is updated by (2.21). The total operation count is $O(N \log_2 N)$. Note that the conformal map is uniquely defined by (2.21) and the supplementary conditions $a_0 = 0$, $\mathrm{Im}(a_1) = 0$. The first condition ensures that the origin of the unit circle is mapped on to the origin of the z plane while the second fixes the overall phase of the map.

As a test of this time dependent mapping method, we study the propagation of Stokes' permanent water waves. In a frame of reference moving with the wave speed, the numerically calculated profiles should be steady. The initial conditions for the calculation are obtained using Padé approximants of perturbation expansions of the Stokes waves [11]. The time-dependent equations (2.21), (2.22) are solved by a fourth-order Adams–Moulton predictor–corrector scheme.

As with other simulations of propagating nonlinear water waves [2, 9], an instability of the free surface quickly develops causing the interface to take on a jagged appearance. The instability is not due to roundoff or time stepping errors and may be physical in origin [9]. To remove the instability the five point smoothing operator used by Longuet-Higgins and Cokelet was employed periodically in our numerical simulation.

For a Stokes wave with peak-to-trough amplitude 80% of the maximum allowed by theory, we choose the time step to be $2\pi/400$ with wavelength 2π and apply smoothing every tenth step. The resulting wave profile is plotted in Fig. 2. The dots indicate the position of the points z_j used to calculate the conformal map of the wave. The solid line is the wave profile computed by Padé approximants [11], translated by an amount to the nonlinear phase speed multiplied by the time. The computation time for one evaluation of the time derivatives of the map and potential is 3 msec on the

CRAY-1 computer using $N = 64$ points. The total computation time for the motion of the wave through one period is about 1 sec. We observe no degradation in the conformal map if the simulation of the Stokes wave is carried out for times longer than one period. However, time stepping errors can cause modulation of the steady wave for times longer than $t = 4\pi$.

The conformal mapping method described here works well provided the region is not highly distorted. As the region of interest becomes more distorted the points corresponding to the conformal map tend to crowd [3, 10]. For example, consider the conformal mapping from the unit disk to the region lying below $y = A \cos kx$. The number of terms N that must be retained in the Fourier expansion (2.4) to obtain a good representation of this map satisfies $\ln N \sim \gamma kA$ as $kA \to \infty$ [3], where $\gamma = (\pi/2) \int_0^\pi ((\sin x)/x)\, dx \simeq 2.909$, showing the difficulty of mapping from the unit disk to a deformed region.

When N is large, almost all of the equally spaced points $e^{i\sigma j}$ on the unit circle are mapped into points z_j that are crowed into small intervals on the boundary of the domain D. Dubiner [3] has recently made a detailed analysis of this problem and has shown that the crowding occurs whenever the region being mapped has a "narrow" section. This effect occurs in high amplitude Rayleigh–Taylor instability and in breaking waves. The FFT method is not effective in dealing with these highly distorted geometries.

When the domain D is highly deformed, the iterative methods [4–8] and our differential equation method do give a conformal map of the unit disk onto a domain that passes through the desired points z_j of ∂D. However, unless N is unreasonably large, the conformal map so obtained will have large deviations from ∂D between the points z_j. Indeed, (2.8) gives an accurate conformal map of ∂D only if a_k decreases rapidly as k increases to $\frac{1}{2}N$.

One possible approach to the crowding problem is to use a sequence of mappings of the disk onto successively more highly deformed regions. Such iterated mappings are still under study. For such methods, one result seems assured, namely that the operation counts must degrade from $O(N \log_2 N)$ to $O(N^2)$ or worse. In this case, these Fourier series methods are probably inferior to the methods to be described in Section 3.

3. Application of the Menikoff–Zemach Method

The Fourier series methods for mapping the unit disk onto D can not accurately handle highly distored domains as the crowding phenomenon causes a severe loss of resolution in some part of the physical boundary. This difficulty may be overcome by mapping D onto the unit disk with a regular distribution of points on ∂D. The crowding then occurs on the boundary of the unit disk. Even with a highly nonuniform distribution of points on the unit circle, the potential problem in the unit disk is still readily solved by Poisson's formula.

Recently, Menikoff and Zemach [10] have developed a new nonlinear integral equation for conformal mapping of the region R above $y=\eta(x)$ onto the periodic semi-infinite strip S: $0\leqslant u<2\pi$, $0\leqslant v<\infty$. Their method requires relatively few points to achieve accurate results for distorted domains.

A simple extension of Menikoff and Zemach's equation which is valid for general periodic interfaces is derived here and is used to investigate the crowding phenomenon for multivalued (or "breaking wave") interfaces. A time dependent version of the equation is also developed. This approach reduces to the integration of N nonlinear differential equations.

The Menikoff–Zemach equations, generalized to handle conformal maps of a domain with boundary curve parametrized as $x=x(e)$, $y=y(e)$, are

$$y(e)=y_\infty+2\int_0^{2\pi}\ln\left|\frac{\sin\frac{1}{2}(u(e)-u(e'))}{\sin\frac{1}{2}(e-e')}\right|\frac{dx}{de'}(e')\frac{de'}{2\pi}$$
$$+\int_0^{2\pi}\cot\left(\frac{e-e'}{2}\right)[(x(e')-e')-(x(e)-e)]\frac{de'}{2\pi}, \tag{3.1a}$$

$$u(e)=x(e)-x_\infty+2\int_0^{2\pi}\ln\left|\frac{\sin\frac{1}{2}(u(e)-u(e'))}{\sin\frac{1}{2}(e-e')}\right|\frac{dy}{de'}\frac{de'}{2\pi}$$
$$+\int_0^{2\pi}\cot\left(\frac{e-e'}{2}\right)[y(e')-y(e)]\frac{de'}{2\pi}. \tag{3.1b}$$

Here e is chosen so that $x(0)=0$, $x(2\pi)=2\pi$, $u(e)$ is defined so $(x(e), y(e))$ is mapped into $(u(e), 0)$, and y_∞, x_∞ are determined by the condition that $u(0)=0$. Note that (3.1a) and (3.1b) are equivalent; either one can be used to determine $u(e)$. Once $u(e)$ is found by solution of (3.1), the conformal map is determined.

Equations (3.1) are derived from the pair of Hilbert transforms:

$$\mathrm{Re}[G(u,0)]=\mathrm{Re}(G_\infty)-P\int_0^{2\pi}\cot\left(\frac{u-u'}{2}\right)\mathrm{Im}[G(u',0]\frac{du'}{2\pi}, \tag{3.2a}$$

$$\mathrm{Im}[G(u,0)]=\mathrm{Im}(G_\infty)+P\int_0^{2\pi}\cot\left(\frac{u-u'}{2}\right)\mathrm{Re}[G(u',0)]\frac{du'}{2\pi}, \tag{3.2b}$$

where $G(W)$ is analytic in the upper-half W-plane and $G(W)=G_\infty+O(1/|W|)$ as $|W|\to\infty$. Equation (3.1) follows if $G=x+iy-W$, where $W=u+iv$.

The Hilbert transforms (3.2) are also useful for solving potential problems in the region R. If the map function $u(e)$ is known, boundary values of a potential ϕ on ∂R may be related to corresponding boundary values of a potential Φ defined in the strip S in the W-plane:

$$\Phi(u) = \phi(e),$$
$$\left.\frac{\partial \Phi}{\partial u}\right|_{v=0} = \frac{\partial \phi}{\partial s}\frac{ds}{de}\Big/\frac{du}{de}, \tag{3.3}$$
$$\left.\frac{\partial \Phi}{\partial v}\right|_{v=0} = \frac{\partial \phi}{\partial n}\frac{ds}{de}\Big/\frac{du}{de},$$

where s and n are the tangential and normal directions to ∂R. The tangential and normal derivatives of Φ are the real and imaginary parts of an analytic functions in S so they are related by the Hilbert transform:

$$\frac{\partial \phi}{\partial n}\frac{ds}{de} = -\int_0^{2\pi} \cot\frac{1}{2}(u(e) - u(e')) \times \left[\frac{d\phi}{de}(e')\frac{du}{de}(e) - \frac{d\phi}{de}(e)\frac{du}{de}(e')\right]\frac{de'}{2\pi}. \tag{3.4}$$

Note that in the application of (3.4) it is necessary to compute du/de with some care. We have found it best to find du/de by using the Hilbert transform of $\ln dz/dw$ to obtain an equation for $\ln du/de$.

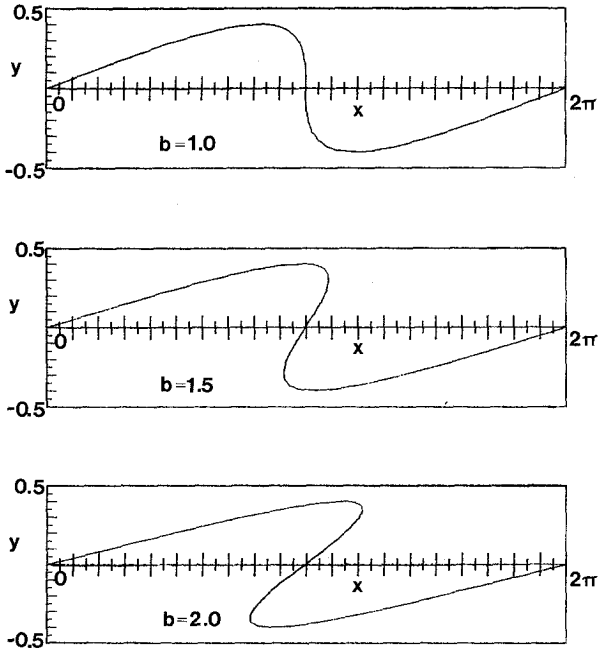

FIG. 3. A plot of y vs x for the "breaking" curves (3.5), $x = e + b \sin e$, $y = 0.4 \sin e$, for $b = 1.0$, 1.5, 2.0.

In order to examine the crowding properties of domains bounded by breaking waves, we use (3.1) to compute the function $u(e)$ for the periodic curve

$$\begin{aligned} x(e) &= e + b \sin e, \\ y(e) &= 0.4 \sin e. \end{aligned} \tag{3.5}$$

For $b < 1$, the curve is a single valued function of x. For $b = 1$, the curve has a vertical slope at $e = \pi$, and for $b > 1$, the function is multivalued. In Fig. 3, the curves (3.5) are plotted for $b = 1$, 1.5, and 2.0. The map function $u(e)$ must be a monotonically increasing function of e. Therefore $du/de > 0$ although it can be exponentially small due to crowding. The functions $u(e)$ and du/de are tabulated for the curves (3.5) in Table I. Another measure of the crowding is given by $\ln(du/de)$. In Fig. 4, $\ln(du/de)$ is plotted for various values of b to reveal the exponential nature of the crowding phenomenon. As b increases, the crowding rapidly becomes severe even though the amplitude of the wave (3.5) is quite modest. Similar crowding should be expected in any dynamic simulation of a breaking wave.

It is also possible to formulate a set of differential equations based on the Menikoff–Zemach approach to map a time-dependent boundary. For parametrized boundaries of the form $(x(e, t), y(e, t))$, the mapping function $u(e, t)$ is determined by

$$\begin{aligned} \frac{\partial u}{\partial t} = \frac{du_0}{dt} &+ \frac{\dfrac{\partial x}{\partial t}\dfrac{\partial x}{\partial e} + \dfrac{\partial y}{\partial t}\dfrac{\partial y}{\partial e}}{\left(\dfrac{ds}{de}\right)^2}\frac{\partial u}{\partial e} \\ &+ \int_0^{2\pi} \cot\left(\frac{u(e) - u(e')}{2}\right)\left[\frac{\dfrac{\partial y}{\partial t}(e')\dfrac{\partial x}{\partial e}(e') - \dfrac{\partial x}{\partial t}(e')\dfrac{\partial y}{\partial e}(e')}{\left(\dfrac{ds}{de}(e')\right)^2}\right. \\ &\left. - \frac{\dfrac{\partial y}{\partial t}(e)\dfrac{\partial x}{\partial e}(e) - \dfrac{\partial x}{\partial t}(e)\dfrac{\partial y}{\partial e}(e)}{\left(\dfrac{ds}{de}(e)\right)^2}\right]\left(\frac{\partial u}{\partial e}(e')\right)^2 \frac{de'}{2\pi}, \end{aligned} \tag{3.6}$$

where $(ds/de)^2 = (\partial x/\partial e)^2 + (\partial y/\partial e)^2$ and $u_0(t)$ is chosen so that $u(0) = 0$.

Given the values of u, ϕ, x, and y at some time t the time stepping algorithm proceeds as follows: First, the values of $u(e)$, $x(e)$ and $y(e)$ are used to determine the map derivative du/de. Next, the normal velocities $\partial\phi/\partial n$ can be computed from (3.4). One $\partial\phi/\partial s$ and $\partial\phi/\partial n$ are known, the boundary curve $(x(e, t), y(e, t))$ can be marched to the next time step. Then, Bernoulli's equation (1.2) gives the boundary values of ϕ at the next step. Finally, Eq. (3.6) is used to march u forward in time.

TABLE I

Mapping Functions for the "Breaking" Curves (3.5)[a]

	$b = 1.0$		$b = 1.5$		$b = 2.0$	
e	$u(e)$	du/de	$u(e)$	du/de	$u(e)$	du/de
0	0.0	1.9239	0.0	2.3575	0.0	2.7670
$\pi/4$	1.5706	1.9648	1.8956	2.3030	2.2126	2.6351
$\pi/2$	2.9331	1.4326	3.4076	1.4615	3.8677	1.4772
$3\pi/4$	3.7681	7.0083×10^{-1}	4.1579	4.9413×10^{-1}	4.5352	3.0688×10^{-1}
π	4.0981	2.0146×10^{-1}	4.3291	4.7511×10^{-2}	4.6125	4.5852×10^{-3}
$5\pi/4$	4.1841	7.7401×10^{-2}	4.3387	6.4110×10^{-4}	4.6131	9.8707×10^{-7}
$3\pi/2$	4.4406	4.2459×10^{-1}	4.3440	4.0460×10^{-2}	4.6131	3.2512×10^{-5}
$7\pi/4$	5.2656	1.2741	4.7624	1.3178	4.6920	7.0508×10^{-1}

[a] The results were checked for 32 and 64 points and agreed to the five significant digits given here.

We have tested the time dependent mapping equation (3.6) on the mapping of the region bounded by a cosine curve of increasing amplitude,

$$\begin{aligned} x(e, t) &= e, \\ y(e, t) &= t \cos(e), \end{aligned} \tag{3.7}$$

and on the regions bounded by a time dependent version of the breaking curves (3.5),

$$\begin{aligned} x(e, t) &= e + t \sin e, \\ y(e, t) &= 0.4 \sin e. \end{aligned} \tag{3.8}$$

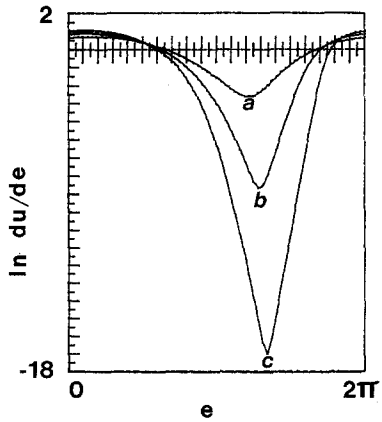

FIG. 4. A plot of $\ln du/de$ for the breaking curves plotted in Fig. 3. (a) $b = 1.0$, (b) $b = 1.5$, (c) $b = 2.0$. Here the Menikoff–Zemach equation (3.1) is solved for the conformal mapping function $u(e)$. Observe the exponentially strong crowding for $b > 1$.

TABLE II

Error in the Conformal Mapping of the Time-Dependent Cosine Curves (3.7)[a]

t	Min(du/de)	Maximum error (percentage)		
		$N=32$	$N=64$	$N=128$
1.0	2.23×10^{-1}	1.8×10^{-5}	3.0×10^{-10}	6.9×10^{-10}
2.0	2.54×10^{-2}	9.1×10^{-2}	2.8×10^{-5}	1.2×10^{-8}
3.0	2.19×10^{-3}	6.9	3.1×10^{-2}	7.4×10^{-7}
4.0	1.66×10^{-4}	—	1.3	3.5×10^{-4}
5.0	1.20×10^{-5}		9.9	2.1×10^{-2}

[a] The time step is $\Delta t=0.001$.

A fourth-order Adams–Moulton predictor–corrector scheme was used to march the map function $u(e,t)$ forward in time. At the times tabulated in Tables II and III, the mapping function was corrected by solving (3.1). The time integration was then restarted with the corrected values of $u(e)$. The maximum error for a given time is given in Tables 2 and 3 for 32, 64, and 128 points. The minimum of the function du/de for each time is also listed to give an indication of the crowding. The error for moderate distortions was fairly insensitive to reductions in the time step Δt but was reduced markedly when the number of points was increased. In regions of severe crowding the time step must be very small in order to ensure accuracy for an explicit integration scheme. Too large a time step can destroy the monotonicity of $u(e)$.

We have also applied the integral equation (3.1) and time-dependent evolution equation (3.6) to the numerical simulation of Rayleigh–Taylor instability. The initial conditions for a single frequency Rayleigh–Taylor problem are as follows. Fluid of density 1 lies above the periodic interface

$$y(e,t=0)=0.5\cos(e),$$

$$x(e,t=0)=e,$$

TABLE III

Error in the Conformal Mapping of the Time-Dependent "Breaking" Curves (3.8)[a]

r	Min(du/de)	Maximum error (percentage)		
		$N=32$	$N=64$	$N=128$
0.8	1.85×10^{-1}	4.5×10^{-5}	3.2×10^{-10}	1.6×10^{-10}
1.0	7.48×10^{-2}	2.0×10^{-3}	3.1×10^{-7}	3.8×10^{-10}
1.2	1.63×10^{-2}	3.9×10^{-2}	9.0×10^{-5}	6.4×10^{-10}
1.4	1.99×10^{-3}	—	4.9×10^{-3}	8.5×10^{-7}
1.6	1.02×10^{-4}	—	—	9.5×10^{-5}

[a] The time step is $\Delta t=0.001$ and 48-bit mantissa arithmetic is used.

and is initially at rest. Below the interface, there is a vacuum. The resulting flow is unstable under gravitational acceleration. The results plotted in Fig. 5 are obtained using the integral equation (3.1). With 60 points per wavelength, we were unable to continue the calculation past a time of $t \simeq 3.5$ at which the amplitude to wavelength ratio of the spike (at $x = \pm\pi$) is about $5.4/2\pi \simeq 0.86$. The degree to which the total energy and the rate of mass flux are conserved gives a good indication of the reliability of the simulation. After a time of 3.0, there is a progressive degradation of conservation of these quantities. This deterioration is also reflected in the spike acceleration. For large t, the spike should be nearly in free fall with an acceleration of -1.0 in our units [1]. In contrast, the present simulation shows a spike acceleration which decreases (in absolute value) below 1.0 after $t = 3.0$. Hence we conclude that the results are not reliable beyond $t = 3.0$. Similarly, the time-dependent evolution equation (3.6) gives results for this problem that are reliable only until $t \simeq 3.0$.

The initial conditions for a multiple frequency Rayleigh–Taylor instability are as follows. Fluid of density 1 lies above the interface with an initial surface deformation of the form

$$y(e, t = 0) = 0.1 \cos e + 0.01 \cos 5e,$$
$$x(e, t = 0) = e,$$

and is again at rest initially. This problem has been previously studied using other methods by White [12] and Baker *et al.* [2]. We obtain the results plotted in Fig. 6 using 60 points. Here, the growth of the short wave spike on the long wave bubble is

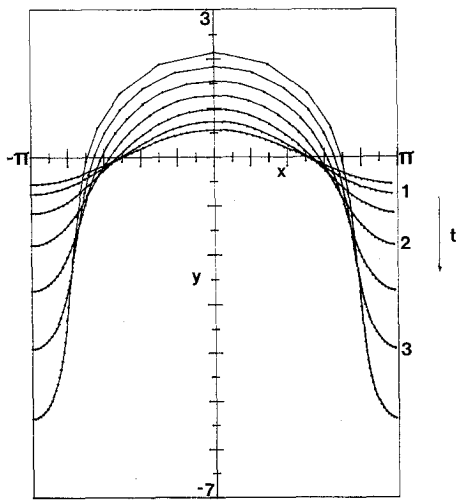

FIG. 5. A plot of the interface $y(x, t)$ for the Rayleigh–Taylor instability with initial conditions $y(x, t = 0) = 0.5 \cos x$, $\phi(x, t) = 0$ for $t = 0.5$ to $t = 3.5$ in steps of 0.5. Here 60 points per wavelength are used. Both the integral equation (3.1) and time-dependent equation (3.6) degrade significantly in accuracy for $t \gtrsim 3$ at this spatial resolution.

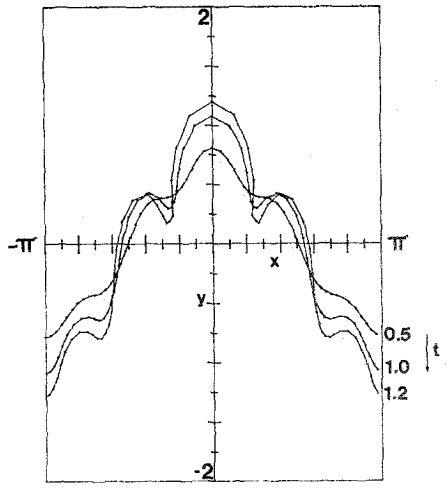

FIG. 6. A plot of the interface $y(x, t)$ for the multifrequency Rayleigh–Taylor instability with initial conditions $y(x, t=0) = 2\pi(0.1 \cos x + 0.01 \cos 5x)$, $\phi(x, t) = 0$ for $t = 0.5$ to 1.2. Here 60 points per wavelength are used. Note that the interface has become multivalued at $t \approx 1.2$. Both the integral equations (3.1) and time-dependent equation (3.6) degrade significantly in accuracy for $t \gtrsim 1.3$ at this spatial resolution.

enhanced relative to the growth of the short wave spike on the long wave spike. This follows from the higher effective gravity in the bubble region. For this initial condition our extension of the Menikoff–Zemach equation must be employed as the interface becomes multivalued after a time of 1.2. The calculation degraded significantly beyond a time of 1.3.

The present conformal mapping methods give results for Rayleigh–Taylor instability that are quite good. The amplitude/wavelength ratio has increased by about a factor 10 for the single frequency run in Fig. 5 before the 60 point calculations degrade. Menikoff and Zemach (private communication) obtain similar amplifications before their calculations break down. However, the reasons for degradation of the calculations at large time remain unclear. On the one hand, the conformal mapping methods described in this Section are capable of resolving much more highly deformed interface than achieved at breakdown, even with 60 points. On the other hand, new vortex methods [1, 2] have been used to calculate the single frequency. Rayleigh–Taylor instability with similar spatial resolution to at least twice the amplifications achieved here. For this reason no smoothing was applied after a time of 3.0 in the Rayleigh–Taylor simulation. It seems that our method of coupling free-surface dynamics and conformal mapping introduces numerical inaccuracies (observed as rapid oscillations of ϕ and η for $t \gtrsim 3.0$). It is possible that this deficiency may be corrected by more sophisticated conformal mapping techniques [3].

REFERENCES

1. G. R. BAKER, D. I. MEIRON, AND S. A. ORSZAG, *Phys. Fluids* **23** (1980), 1485.
2. G. R. BAKER, D. I. MEIRON, AND S. A. ORSZAG, to be published.
3. M. DUBINER, Ph. D. thesis, Department of Mathematics, MIT, Cambridge, Mass., 1981.
4. B. FORNBERG, *SIAM J. Sci. Stat. Comp.*, in press.
5. D. GAIER, "Konstruktive Methoden der Korformen Abbildung," Springer, Berlin, 1964.
6. C. GRAM, "Selected Numerical Methods for Linear Equations, Polynomial Equations, Partial Differential Equations, Conformal Mapping," Regnecentralen, Copenhagen, 1962.
7. D. IVES, *AIAA J.* **14** (1976), 1006.
8. L. V. KANTOROVICH AND V. I. KRYLOV, "Approximate Methods of Higher Analysis," Interscience, New York, 1958.
9. M. S. LONGUET-HIGGINS AND E. D. COKELET, *Proc. Roy. Soc. London Ser. A* **350** (1976), 1.
10. R. MENIKOFF AND C. ZEMACH, *J. Comput. Phys.* **36** (1980), 366.
11. L. W. SCHWARTZ, *J. Fluid Mech.* **62** (1974), 553.
12. G. N. WHITE, Los Alamos Scientific Laboratory Report LA-5575-MS, 1974.